Cross-validation of MIPAS/ENVISAT and GPS-RO/CHAMP temperature profiles

Ding-Yi Wang,[1] Gabriele P. Stiller,[1] Thomas von Clarmann,[1] Herbert Fischer,[1] Manuel López-Puertas,[2] Bernd Funke,[2] Norbert Glatthor,[1] Udo Grabowski,[1] Michael Höpfner,[1] Sylvia Kellmann,[1] Michael Kiefer,[1] Andrea Linden,[1] Gizaw Mengistu Tsidu,[1] Mathias Milz,[1] Tilman Steck,[1] Jonathan H. Jiang,[3] Chi O. Ao,[3] Gloria Manney,[3,4] Klemens Hocke,[5] Dong L. Wu,[3] Larry J. Romans,[3] Jens Wickert,[6] and Torsten Schmidt[6]

Received 28 April 2004; revised 26 July 2004; accepted 5 August 2004; published 9 October 2004.

[1] The Michelson Interferometer for Passive Atmospheric Sounding (MIPAS) on board the ENVISAT and the Global Positioning System (GPS) receiver on the Challenging Mini-Satellite Payload (CHAMP) provide temperature profiles by limb-viewing midinfrared emission and radio occultation (RO) measurements, respectively. The MIPAS temperatures retrieved at the Institut für Meteorologie und Klimaforschung (IMK) are compared with the GPS-RO/CHAMP observations derived at Jet Propulsion Laboratory (JPL) and GeoForschungsZentrum (GFZ) Potsdam. The three data sets show generally good agreement. The global mean differences averaged between 8 and 30 km in 14 days of September/October 2002 are -0.44 ± 0.02 K and 0.07 ± 0.02 K for MIPAS/GPS-RO JPL and GFZ comparisons, respectively. The MIPAS global mean temperatures below 25 km are slightly lower than those of GPS-RO JPL and GFZ by less than 1 K and 0.2 K, respectively. Above 25 km, the MIPAS temperatures are higher than the JPL and GFZ data, in particular near both poles and the equator, with maxima of 1 K for JPL and 1.5 K for GFZ at 30 km. The standard deviations are $\sim$2–4 K. Possible explanations for the observed differences include (1) effect of spatial and temporal mismatch between the correlative measurements on the observed standard deviations, in particular in regions and episodes of enhanced wave activity; (2) a negative bias in GPS-RO/CHAMP temperatures in regions of increased humidity; (3) a mapping of initialization temperature profiles on GPS-RO/CHAMP retrievals at altitudes where low refraction contains no information on air density; and (4) measurement errors of both instruments, particularly the errors due to insufficient knowledge of the instrument line shape and spectroscopy in current MIPAS retrievals. *INDEX TERMS:* 0394 Atmospheric Composition and Structure: Instruments and techniques; 3360 Meteorology and Atmospheric Dynamics: Remote sensing; 3394 Meteorology and Atmospheric Dynamics: Instruments and techniques; *KEYWORDS:* CHAMP, MIPAS, temperature

Citation: Wang, D.-Y., et al. (2004), Cross-validation of MIPAS/ENVISAT and GPS-RO/CHAMP temperature profiles, *J. Geophys. Res.*, *109*, D19311, doi:10.1029/2004JD004963.

1. Introduction

[2] Reliable information on global climate change processes over future decades, and the potential need for improved weather forecasting on short- and medium-term timescales, are only possible on the basis of global and regional data records and modeling that accurately represent atmospheric state parameters with high spatial and temporal resolution.

[3] The Michelson Interferometer for Passive Atmospheric Sounding (MIPAS) on the ENVISAT satellite measures vertical profiles of tropospheric and stratospheric temperature and volume mixing ratio (VMR) of various gas species by limb-observing midinfrared emissions [*Fischer and Oelhaf*, 1996; see also *European Space Agency* (*ESA*), 2000]. In addition to the ESA operational data processing, there are six different processors at five institutions for science-oriented data analysis of the high resolution radiometric spectra. A blind test retrieval experiment based on synthetic spectra [*von Clarmann et al.*, 2003b] and a

[1]Institut für Meteorologie und Klimaforschung (IMK), Forschungszentrum Karlsruhe GmbH und Universität Karlsruhe, Karlsruhe, Germany.
[2]Instituto de Astrofísica de Andalucía, CSIC, Granada, Spain.
[3]Jet Propulsion Laboratory, California Institute of Technology, Pasadena, California, USA.
[4]Department of Natural Sciences, New Mexico Highlands University, Los Vegas, New Mexico, USA.
[5]Max-Planck-Institut für Aeronomie, Katlenburg-Lindau, Germany.
[6]Department 1: Geodesy and Remote Sensing, GeoForschungsZentrum Potsdam (GFZ), Potsdam, Germany.

0148-0227/04/2004JD004963$09.00

comparison of retrievals from four orbits of real measurements [*Steck*, 2003] have shown that all the data processors are capable of producing reliable results within their individual specifications.

[4] The MIPAS data analysis processor at Institut für Meteorologie und Klimaforschung (IMK) provides simultaneous retrievals of temperature and line-of-sight parameters from measured spectra and the spacecraft ephemerides. Also, atmospheric pressure is indirectly registered through hydrostatic equilibrium. This step precedes the species abundance retrievals, since an accurate knowledge of the observational geometry and the physical state of the atmosphere is an essential requirement for any space-based limb-viewing remote sensing experiment attempting to characterize the chemical composition of our environment. The details of the current retrieval scheme and its robustness and accuracy have been discussed by *von Clarmann et al.* [2003a, 2003b, 2003c] and *Stiller et al.* [2003a, 2003b].

[5] The Global Positioning System (GPS) radio occultation (RO) technology is developing into a powerful tool for continuously monitoring the atmosphere and providing data complementary to other sounding techniques, such as multispectral passive radiometers [*Gorbunov and Sokolovskiy*, 1993; *Melbourne et al.*, 1994; *Ware et al.*, 1996; *Kursinski et al.*, 1997]. Meteorologists are looking forward with high expectations to this new technique because of their need for an operationally reliable, high resolution global data base to produce reliable weather forecasts by applying data assimilation and numerical modeling techniques [e.g., *Wickert et al.*, 2004a, 2004b]. The recently launched polar orbiting German Challenging Mini-Satellite Payload (CHAMP) for Geoscientific Research and Application and Argentinian Satelite de Aplicaciones Cientificas-C (SAC-C) carry with them the new-generation GPS receiver, the ''BlackJack''-supplied by the Jet Propulsion Laboratory (JPL). Since 2001 the receivers have collected occultation data and provided profiles of refractivity, temperature, pressure and water vapor in the neutral atmosphere, and electron density in the ionosphere.

[6] The GPS-RO/CHAMP data are processed at the GeoForschungsZentrum Potsdam (GFZ, Germany), JPL, and University Corporation of Atmospheric Research (UCAR), as well as other institutions using different approaches. Due to different treatment on water vapor component, the derived GFZ and JPL data represent ''dry'' and ''wet'' temperatures, respectively. Also, to derive atmospheric density (thus temperature) and humidity profiles from the calculated refractivity, the GFZ and JPL data processor use different a priori temperature profiles to initialize the hydrostatic equation at different height levels. Statistical comparisons of several thousands CHAMP GFZ temperature measurements with radiosonde data (with coincidence criteria of horizontal distance less than 300 km and time difference less than 3 hours) showed mean deviation of -0.1 to -0.4 K and standard deviations less than 2 K above 8 km and below 30 km. At 30 km a negative bias of $\sim$1 K for the CHAMP retrievals is reported for these comparisons [*Wickert et al.*, 2004a, 2004b]. Comparison between vertical profiles of dry temperature derived by GFZ and UCAR shows no statistically significant differences [*Wickert et al.*, 2001a, 2003]. The refractivities derived by GFZ, JPL, and UCAR are generally in good agreement [*Wickert et al.*, 2003; *Ao et al.*, 2003]. The CHAMP and SAC-C JPL profiles occurring within 30 min and 200 km are compared and agreed to better than 0.86 K (68% confidence interval) and to within 0.1 K in the mean between 5 and 15 km altitude, after removing the expected variability of the atmosphere [*Hajj et al.*, 2004].

Table 1. Numbers of Coincidence Profiles Used for Comparison[a]

Time	MIPAS Total	CHAMP Total	MIPAS/CHAMP
18 Sept. 2002	479	138	80/89
19 Sept. 2002	514	136	87/101
20 Sept. 2002	480	152	100/108
21 Sept. 2002	384	154	77/91
22 Sept. 2002	412	154	83/91
23 Sept. 2002	214	157	30/37
24 Sept. 2002	213	152	38/44
25 Sept. 2002	232	153	59/64
26 Sept. 2002	475	127	59/64
27 Sept. 2002	568	137	95/113
28 Sept. 2002	30	119	8/8
11 Oct. 2002	292	130	57/67
12 Oct. 2002	292	132	47/50
13 Oct. 2002	509	141	103/115

[a]Coincidence criteria: For the individual paired profiles, latitude and longitude differences are smaller than 5 and 10 degrees, respectively. The time differences are less than 6 hours. The second and third columns are numbers of available MIPAS and GPS-RO CHAMP measurements on each day, respectively, and the fourth column is the number of their correlative profiles.

[7] Extensive validation campaigns and error analyses for both observation systems will produce definite statements about the reliability and utility of these data. Of long-term and strategic importance, this will establish basic conditions for their use in operational meteorology. The MIPAS IMK temperatures have previously been compared with the GPS-RO/CHAMP GFZ data [*Wang et al.*, 2004a] and the GPS-RO/SAC-C measurements [*Jiang et al.*, 2004a], as well as with a number of other satellite observations [*Wang et al.*, 2004b]. They found that the MIPAS IMK temperatures showed good consistency with those of the GPS-RO/CHAMP GFZ and SAC-C data during the stratospheric major sudden warming in the southern hemisphere winter of 2002, with the overall mean differences and standard deviations estimated at $\sim$1 K and $\sim$5 K, respectively.

[8] In this study, we compare the GPS-RO/CHAMP temperatures produced by the JPL and GFZ processors with the MIPAS IMK data. This comparison benefits not only the two different limb-viewing observation systems of active radio occultation and passive infrared emission, but also the two different approaches of GPS-RO/CHAMP data processing at JPL and GFZ, in order to evaluate the methods and to assess their effectiveness. Our comparison method and the characteristics of the MIPAS and GPS-RO data are described in section 2. The comparisons between the MIPAS and GPS-RO temperature profiles are displayed in section 3. Possible reasons for detected differences are discussed in section 4. Our conclusions are contained in section 5.

2. Data and Comparison Method

[9] The MIPAS temperatures used for this study are taken from the observations during 14 days in September/October of 2002 (see the first column of Table 1). The data are IMK product version V1.0. They are derived from limb-viewing

infrared emissions by the IMK data processor using the standard retrieval approach of constrained nonlinear multi-parameter least squares fitting. The MIPAS observations from ENVISAT, the sun-synchronous polar orbiter, provide global coverage with 14.4 orbits per day. At a given latitude over the course of a day, about 30 longitudinal points are sampled, 15 each in the ascending and descending nodes. The local solar time across the equator is 10:00 and 22:00 in the descending and ascending nodes, respectively. The data points in each node have approximately constant local time at a given latitude, and slightly different local times at different latitudes. The standard observation mode covers tangent altitudes between 6 and 42 km at step width of 3 km, then 47, 52, 60, and 68 km. The measurement spacing is ~500 km along-track and ~2800 km across-track at the equator. The temperature data are retrieved from the operational ESA level-1B version V4.53 data (i.e., calibrated and geo-located radiance spectra). The European Centre for Medium-Range Weather Forecasts (ECMWF) operational analyses of temperature are used as initial guess. The retrieval of current version V1.0 is performed between 6 and 70 km on a 1-km grid below 44 km and 2-km above. Because the retrieval grids are finer than the typical vertical distance of two adjacent tangent points, the solution must be stabilized by a constraint. A Tikhonov-type smoothing constraint has been chosen as discussed by *von Clarmann et al.* [2003c] and resulted in typical altitude resolution of 3–4 km. More features of the retrievals as characterized by the averaging kernel will be discussed in the next section. The bottom and top of the atmosphere are taken to be the Earth's surface and 120 km, respectively. This choice eliminates lower and upper boundary effects on retrieved temperatures at altitudes of 6–68 km where one can reasonably expect quality retrievals. Also, local thermodynamic equilibrium (LTE) is assumed in the retrievals, since the non-LTE effects are not significant in the region below 70 km except for the lower mesosphere in the polar winter regions [*von Clarmann et al.*, 2003c]. Some measurements with severe cloud contamination were rejected (see *Spang et al.* [2004] for details of the cloud-clearing technique). The number of available measurements for each day varies from several tens to hundreds (see the second column of Table 1). The total (including systematic and noise) error of MIPAS temperature measurements is estimated at 0.5–1.5 K, varying from profile to profile, with the larger value for the lowest and highest levels of the observation range [*von Clarmann et al.*, 2003c]. Further description of the data and retrieval techniques can be found in *von Clarmann et al.* [2003a, 2003b, 2003c] and *Stiller et al.* [2003a, 2003b].

[10] GPS-RO/CHAMP temperatures are taken from the level 2 data product JPL version V1.0 and GFZ version 4. CHAMP is a low Earth orbiter (LEO). The GPS-RO observation locations are relatively evenly spaced. The measurements provide about 200 globally distributed vertical profiles of atmospheric parameters per day within the height interval of 0–50 km. Currently JPL provides temperature retrievals up to 30 km, and GFZ up to 35 km, with a measurement error of ~1 K. The vertical resolution ranges from 0.5 km in the lower troposphere to 1.5 km in the stratosphere and the resolution along the ray path is a few hundred kilometers. The phase delays of the GPS carrier signals induced by the intervening medium can be accurately measured as the GPS-LEO satellite link descends through the atmosphere. Knowing the geometry of the occultation, i.e., position and velocity of both satellites, the bending angle of each ray can be derived assuming a spherical atmosphere. The bending angle measurements can be directly inverted through the Abel transform to yield the refractive index profile. Coupled with the hydrostatic equation, the refractivity profile can be converted unambiguously into a temperature profile above the tropopause, where the water vapor contribution is small [*Thayer*, 1974]. At microwave frequencies the refractivity is very sensitive to water vapor. When water vapor is present, additional information is required to determine the humidity and density from refractivity profiles. In the GFZ and JPL GPS-RO data processor, temperature profiles from the ECMWF and NCEP (National Centers for Environmental Prediction) analysis are used to initialize the hydrostatic equation at 43 km and 30 km, respectively, and to derive humidity and atmospheric density (thus temperature) profiles from the calculated refractivity in an iterative procedure [*Gorbunov and Sokolovskiy*, 1993]. The derived GPS-RO temperatures depend on the initialization at these altitudes [*Wickert et al.*, 2001b; *Marquardt et al.*, 2003]. If one compares the GFZ or JPL retrievals with the ECMWF or NCEP at 43 km or 30 km, respectively, zero bias and standard deviation (pure ECMWF or NCEP) are expected. This feature is not associated with the measurement principles, but simply due to the very straightforward manner of using the initialization information in the current retrieval scheme. The CHAMP temperature and water vapor profiles also can be derived by using optimal estimation methods from the observed refractivity. The implementation of appropriate algorithms is currently under investigation. Detailed descriptions of the retrieval algorithm can be found in the works of *Gorbunov and Sokolovskiy* [1993], *Melbourne et al.* [1994], *Kursinski et al.* [1997], *Hocke* [1997], *Steiner et al.* [1999], *Palmer et al.* [2000], and *Hajj et al.* [2002].

[11] Owing to characteristics of the sampling scenarios for the two instruments, it is difficult to achieve good spatial and temporal coincidence between individual MIPAS and GPS-RO measurements. Thus, as a first approximation, the overlapped profile comparisons are conducted for those measurements with latitude and longitude differences smaller than 5° and 10°, respectively, with time differences constrained to less than 6 hours. The coincidence criteria result in maximum separation distances of ~1200 km around the equator and ~700 km near both poles. Figure 1 shows the mean spatial and temporal differences and their standard deviations averaged over 30° latitude intervals for the coincidence events selected from the MIPAS descending orbit observations during the 14 days of September/October 2002. The results for the ascending observations are similar and not shown here. The average separation distances are ~630 ± 300 km and ~350 ± 150 km in the tropical and polar latitude bins, respectively. The average time differences are about −1 or −2 hours with spreads of ~3 hours near the poles, but close to −3 hours with smaller spreads of ~1 hour around the equator. The global averaged separation is about ~450 km with a standard deviation of ~230 km. The global mean differences in latitude and longitude are −0.21 ± 2.88 and 0.03 ± 5.59 degrees, respectively. The global mean time difference is about −2.5 hours with a spread of ~2 hours. These results suggest that the spatial

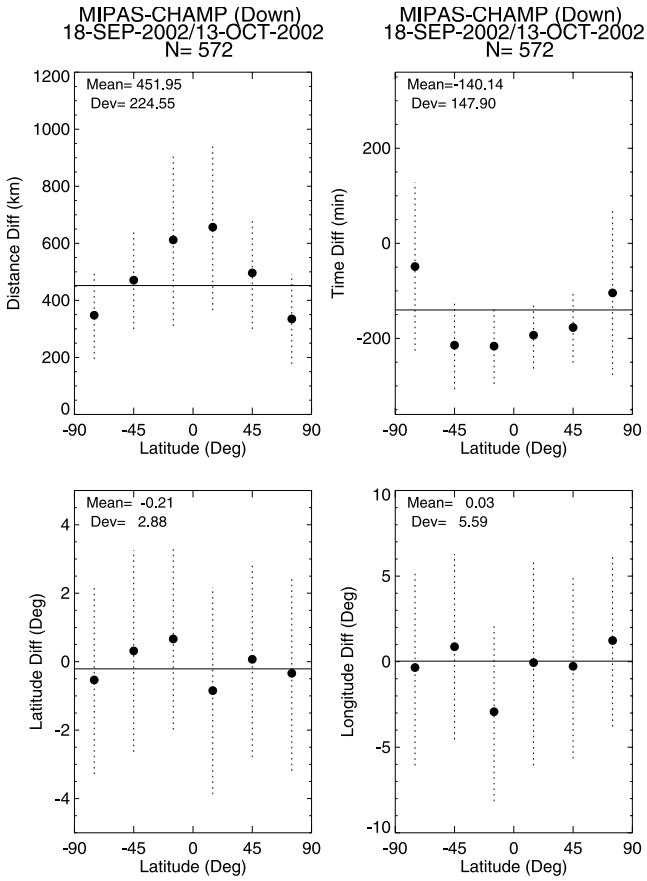

Figure 1. Latitudinal distribution of spatial and temporal differences between the MIPAS and GPS-RO/CHAMP correlative measurements. The differences in horizontal distance (top left) and time (top right) are in kilometers and minutes, respectively. The differences in latitude (bottom left) and longitude (bottom right) are in degrees. Shown are the zonal mean differences (circle) and standard deviations (dotted line) averaged over 30° latitude intervals centered at 15°, 45°, and 75° in both hemispheres. Total 572 coincident profiles are taken from the MIPAS descending orbit observations (daytime) during the 14 days of September/October 2002. The global means and standard deviations of the differences are denoted in each panel.

and temporal mismatches between the correlative measurements are minimized in the polar regions.

[12] The correlative profiles are interpolated to a common altitude grid, that used by the MIPAS-IMK data processor. The GPS-RO data have higher vertical resolution than the MIPAS measurements. Some small structures of the temperature field could be resolved by the higher resolution, but not by the lower one. In account for this effect, adjustment of altitude resolution or averaging kernel must be applied. The method is described by *Rodgers and Connor* [2003], and its simplified application to MIPAS and CHAMP data is outlined below.

[13] When disregarding noise, the retrieved profile $\mathbf{x}_{retrieved}$ is a weighted average of the "true" profile $\mathbf{x}_{true}$ and a priori profile $\mathbf{x}^a$ in the form of

$$\mathbf{x}_{retrieved} = \mathbf{A}\mathbf{x}_{true} + (\mathbf{I} - \mathbf{A})\mathbf{x}^a, \tag{1}$$

where $\mathbf{A}$ is the averaging kernel and $\mathbf{I}$ denotes unit matrix. The vertical resolution of the high-resolved CHAMP profiles $\mathbf{x}_{champ}$ is adjusted by applying the averaging kernel of the low-resolved MIPAS profiles $\mathbf{A}_{mipas}$. Also, the CHAMP profiles, which is assumed to be free of a priori information, are transformed to the a priori of MIPAS $\mathbf{x}^a_{mipas}$. Both the a priori transformation and smoothing is done by

$$\tilde{\mathbf{x}}_{champ} = \mathbf{A}_{mipas}\mathbf{x}_{champ} + \left(\mathbf{I} - \mathbf{A}_{mipas}\right)\mathbf{x}^a_{mipas}. \tag{2}$$

Comparing equation (2) with equation (1), it is clear that $\tilde{\mathbf{x}}_{champ}$ is the result derived with the MIPAS inverse model, if $\mathbf{x}_{champ}$ happens to be the true profile. The significantly higher resolution of the GPS measurements with respect to the MIPAS observations makes meaningful the approximation of considering the GPS measurements as direct measurement of temperature. The difference between $\mathbf{x}_{mipas}$ and $\tilde{\mathbf{x}}_{champ}$ is

$$\begin{aligned}\delta &= \mathbf{x}_{mipas} - \tilde{\mathbf{x}}_{champ} \\ &= \left(\mathbf{x}_{mipas} - \mathbf{x}_{champ}\right) + \left(\mathbf{I} - \mathbf{A}_{mipas}\right)\left(\mathbf{x}_{champ} - \mathbf{x}^a_{mipas}\right),\end{aligned} \tag{3}$$

where the negative of the last term represents the differences originated from different vertical resolution and a priori. These contribute to the $(\mathbf{x}_{mipas} - \mathbf{x}_{champ})$ difference, but not to δ. Thus the residual δ is taken as proxy for the discrepancy between the two measurements. For the ith pair of the correlative profiles, the individual elements of the difference profile vector δ_i at each height level z will be denoted as $\delta_i(z)$ hereafter.

[14] We note that $\delta_i(z)$ provides a comparison between $\mathbf{x}_{mipas}$ and $\mathbf{x}_{champ}$ only in cases where information from the MIPAS measurement is contained in the retrieval, i.e., the diagonal values of $\mathbf{A}_{mipas}$ is reasonably large. If the diagonal values of $\mathbf{A}_{mipas}$ are small, i.e., no altitude-resolved measurement information is contained in the MIPAS retrieval, equation (3) reduces to $\delta = \mathbf{x}_{mipas} - \mathbf{x}^a_{mipas}$, implying a tendency of comparison between $\mathbf{x}_{mipas}$ and its a priori $\mathbf{x}^a_{mipas}$. In this case, since vertical structures in both the MIPAS retrieval and $\tilde{\mathbf{x}}_{champ}$ are dominated by the common a priori $\mathbf{x}^a_{mipas}$, and small $\delta \simeq 0$ do not imply a meaningful agreement between $\mathbf{x}_{mipas}$ and $\mathbf{x}_{champ}$. Figure 2 displays a typical $\mathbf{A}_{mipas}$. In the scaled form, the bright regions correspond to large values and the dark regions to small ones. The matrix is dominated by the diagonal with values of 0.3–0.5, which means that the retrieved temperatures reflect the true profile quite well. However, the smoothing influence of the Tikhonov-type regularization also produces off-diagonal elements in $\mathbf{A}_{mipas}$. The lowest diagonal values of ~0.2 are seen at the tangent heights below 20 km, where the least information about the target parameters is available. Nevertheless, we have diagonal values of $\mathbf{A}_{mipas} \neq 0$ for all altitudes, suggesting that equation (3) provides a meaningful comparison between $\mathbf{x}_{mipas}$ and $\mathbf{x}_{champ}$ in the entire altitude region under consideration.

[15] The covariance of the difference $\delta_i(z)$ is determined by

$$\mathbf{S}_\delta = \left(\mathbf{A}_{mipas} - \mathbf{A}_{champ}\right)^T \mathbf{S}_{mipas}\left(\mathbf{A}_{mipas} - \mathbf{A}_{champ}\right) + \mathbf{S}_{mipas} + \mathbf{S}_{champ}, \tag{4}$$

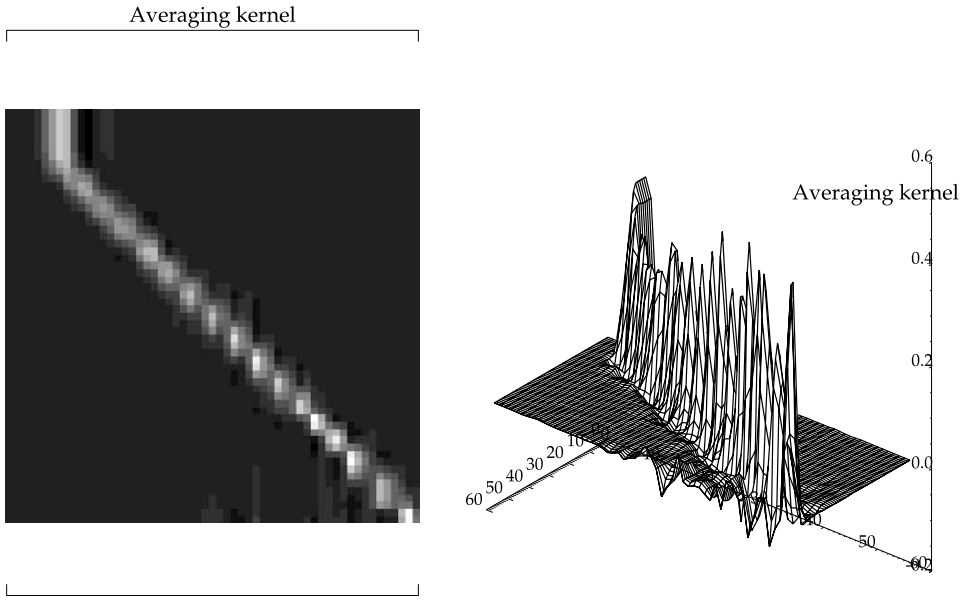

Figure 2. Averaging kernel matrix $\mathbf{A}_{mipas}$ for the MIPAS measurement taken at 07:09:44 UTC on 26 September 2002 (63.13°S and 129.3°W). Displayed are scaled (left) and three-dimensional (right) forms.

where $\mathbf{S}_{mipas}$ and $\mathbf{S}_{champ}$ are the covariances of MIPAS and CHAMP measurements, respectively. However, $\mathbf{S}_{\delta}$ is not estimated in our analysis. The main difficulty in carrying out such task is the lack of knowledge of the a priori, averaging kernels and retrieval error covariance for the two GPS-RO/CHAMP measurements, so that the appropriate expected error covariance of the comparison ensemble cannot be calculated.

[16] The residuals $\delta_i(z)$ are assembled in several ways (details are described in section 3) for statistical analysis. For each ensemble, average difference profiles between the correlative MIPAS and GPS-RO/CHAMP measurements are calculated by

$$\Delta(z) = \frac{1}{N}\sum_{i=1}^{N}\delta_i(z), \tag{5}$$

where $\Delta(z)$ refers to the average difference and $N = N(z)$ to the total number of coincident measurement pairs at a given altitude. To quantify the spread in the individual measurements pairs, the standard deviation of the distribution, $\sigma(z)$, at each altitude is computed by

$$\sigma^2(z) = \frac{1}{(N-1)}\sum_{i=1}^{N}[\delta_i(z) - \Delta(z)]^2. \tag{6}$$

The statistical uncertainty in the mean difference $\Delta(z)$ is quantified by $\sigma(z)/N^{1/2}$, i.e., the 1-σ error [e.g., see *Bevington*, 1969]. This quantity is used as an error bar to characterize the significance of the estimated mean differences between the correlative measurements. The figure represents the uncertainty of $\Delta(z)$ due to random-type errors. In the case of $\Delta(z)$ larger than its statistical 1-σ error, their difference is an indicator of systematic errors between the comparison data sets, at which this study is targeted. We also compute mean difference, standard deviation, and 1-σ uncertainty averaged over altitude. These height-averaged quantities are directly evaluated according to equations (5) and (6) by assembling data points available at all height levels of interest.

3. Comparison Results

[17] Detailed profile comparisons are performed for the MIPAS measurements between 8 and 30 km during September/October 2002. The cutoff altitudes are due to the current version of GPS-RO data. Above 30 km, the influence of the initialization data dominates the derived GPS-RO temperatures (see section 4.3). Below 8 km the presence of water vapor results in larger bias in the retrieved GPS-RO profiles (see section 4.4). The numbers of correlative profiles used for this study are listed in the 4th column of Table 1. The coincidence criteria are defined in the previous section. One MIPAS profile may have multiple GPS-RO/CHAMP coincidences due to the sampling characteristics and our coincidence criteria. The latitude coverage is global for the correlative measurements during the observation period. We assemble sets of comparisons to reduce influences of geophysical variations in the temperature residuals and to judge whether biases are present between the two instruments.

[18] We first compare daily zonal mean profiles of the retrieved MIPAS and GPS-RO/CHAMP temperatures, i.e., $\mathbf{x}_{mipas}$ and $\mathbf{x}_{champ}$. To determine the means, all available longitudinal data at individual heights are sorted into latitude bins of a specified width (30° in latitude is used here to have enough data points available in each bin). The averaged profiles of the MIPAS IMK and GPS-RO/CHAMP JPL temperatures on 26 September 2002 are shown in Figure 3 as an example. The comparisons between the MIPAS IMK and GPS-RO/CHAMP GFZ data exhibit similar features and are not displayed here. Shown in Figure 3 are the retrieved profiles of $\mathbf{x}_{mipas}$ and $\mathbf{x}_{champ}$, i.e., no adjustment of altitude resolution and a priori

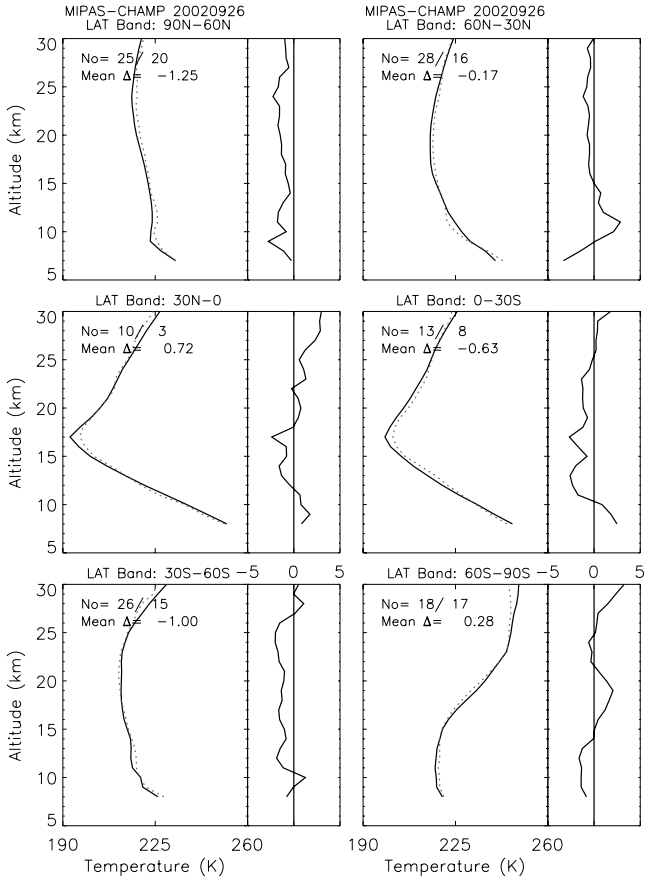

Figure 3. Comparisons of MIPAS IMK (solid) and GPS-RO/CHAMP JPL (dotted) temperatures (in Kelvin) on 26 September 2002. The temperature profiles (left subpanel) $\mathbf{x}_{mipas}$ and $\mathbf{x}_{champ}$ and their differences (right subpanel) $\mathbf{x}_{mipas} - \mathbf{x}_{champ}$ are averaged over available correlative measurements within the specified latitude bands. No adjustment of altitude resolution and a priori information is used. The numbers of data points N vary at individual heights due to data selection (see section 2). The maximum and minimum values of N are denoted, followed by mean differences averaged over all heights.

information is used. In spite of it, the daily zonal mean MIPAS and GPS-RO temperature profiles generally show good agreement. The mean differences between $\mathbf{x}_{mipas}$ and $\mathbf{x}_{champ}$ at individual heights vary between ±(1–2) K, and the mean differences averaged over the height region of 8 and 30 km are between −1.25 and 0.7 K for the six latitude bins. Larger discrepancies are seen in the polar regions of both hemispheres, with the height-averaged mean differences of −1.25 K at 60°N–90°N and −1.0 K at 30°S–60°S. These differences in the polar regions represent the worst case in our comparisons as shown later.

[19] As seen in Figure 3, the MIPAS temperatures $\mathbf{x}_{mipas}$ near the tropical tropopause are lower than the GPS-RO $\mathbf{x}_{champ}$ by ∼3 K in a narrow height region around 17 km. Similar larger discrepancies are also observed around 10 km at other latitude bands. To investigate the origin of the large discrepancies, we apply the adjustment of vertical resolution and a priori information to the CHAMP data (see equation (2)), and compare the transformed CHAMP data $\tilde{\mathbf{x}}_{champ}$ with the retrieved MIPAS data $\mathbf{x}_{mipas}$. The results are displayed in Figure 4, where the discrepancies around the tropopause regions are significantly reduced. This proves that the large discrepancies between $\mathbf{x}_{mipas}$ and $\mathbf{x}_{champ}$ are originated from high-resolution features not resolved by MIPAS. As shown by equation (1) and discussed in the previous section, the MIPAS retrievals have a tendency to conserve the a priori structures in spatial scales smaller than the tangent altitude resolution (∼3 km) [see also *von Clarmann et al.*, 2003b]. The ECMWF temperatures are used as the a priori information in the MIPAS IMK algorithm, and are taken from the ENVISAT validation database NADIR (the NILU Atmospheric Database for Interactive Retrieval) at NILU (Norsk Institutt for Luftforskning). They are currently resampled on standard pressure levels from the ground to 0.1 hPa, including 300, 200, 140, 100, 90, and 70 hPa in the region of our interest. These values correspond to vertical grids of ∼2–3 km in the tropopause regions. Thus the subscale structures around the tropopause are not well resolved in the a priori and MIPAS measurements, and behave as if they were fixed at nearly the same tropopause

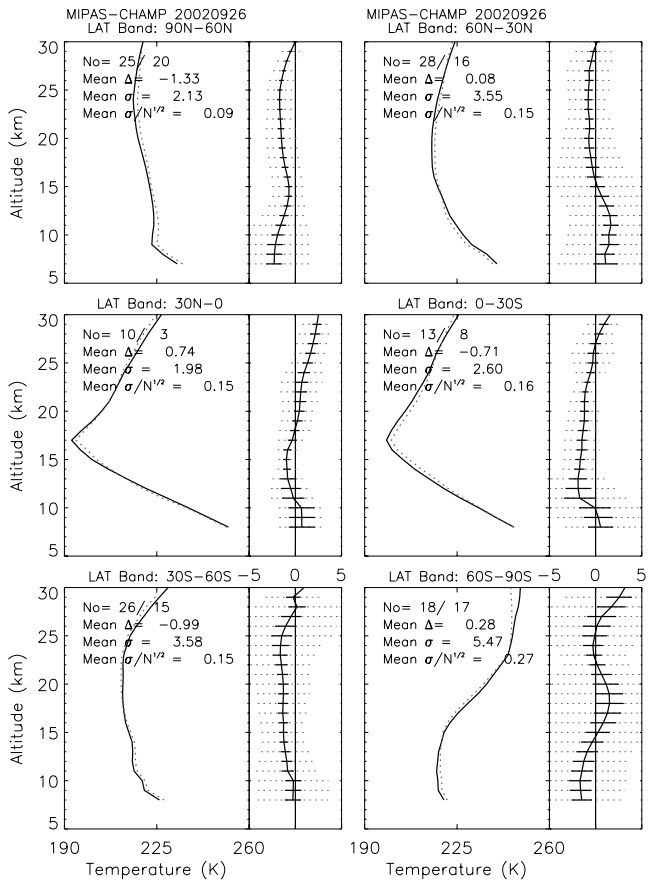

Figure 4. Same as Figure 3, but adjustment of altitude resolution and a priori information is applied to the CHAMP data; i.e., temperature profiles are $\mathbf{x}_{mipas}$ and $\tilde{\mathbf{x}}_{champ}$, and their differences are $\delta = \mathbf{x}_{mipas} - \tilde{\mathbf{x}}_{champ}$. Shown in the right subpanels are the means $\Delta(z)$ and standard deviations $\sigma(z)$, averaged at each height for δ. Denoted in the left subpanel are maximum and minimum values of N at each height level, followed by mean $\Delta(z)$, $\sigma(z)$, and 1-σ error averaged over all heights.

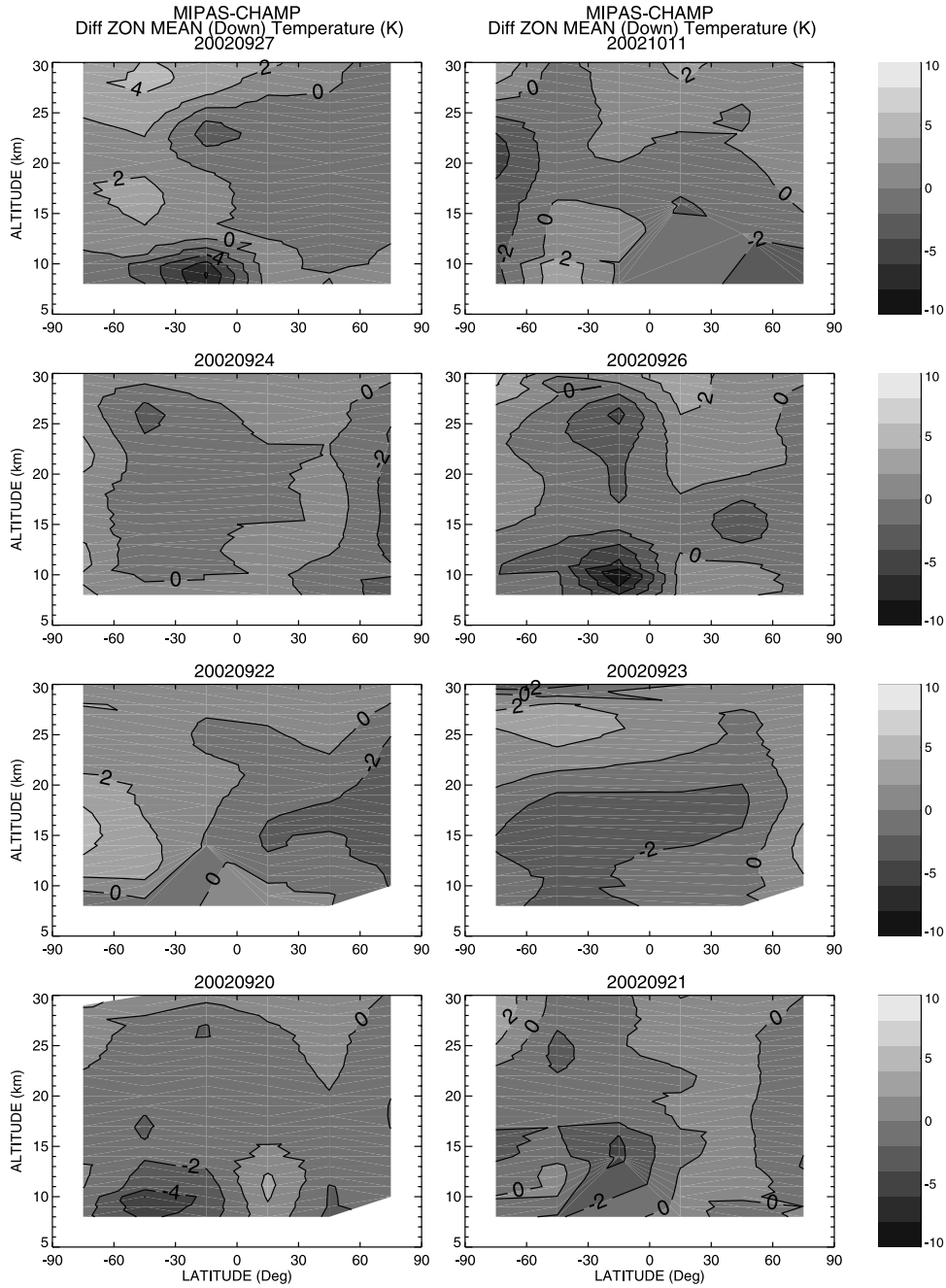

Figure 5. Daily zonal mean temperature differences (in Kelvin) of correlative MIPAS IMK and GPS-RO/CHAMP JPL retrievals. Adjustment of altitude resolution and a priori information is applied. MIPAS observations are in descending orbit node (daytime). See Table 1 for the criteria and numbers of coincidence. The temperature contour interval is 2 K.

altitude. This feature is also mapped into all MIPAS retrievals in that region, resulting in a sharper subscale profile due to little cancellation during averaging. In contrast, CHAMP measurements resolve the tropopause better; i.e., CHAMP can retrieve different tropopause altitudes for individual measurements. After averaging, the resultant profile looks smoother. More discussions about the effect of vertical resolution are presented in section 4.2.

[20] We further examine the daily zonal mean differences between the correlative observations in detail. To eliminate the difference originated from different a priori and vertical resolution, the GPS-RO/CHAMP data are transformed using equation (2) and the difference $\delta_i(z)$ at each height for individual MIPAS/GPS-RO correlative measurements are determined from equation (3). The means of available points in each latitude bin of a 30° width are computed separately for each leg of MIPAS orbit. In doing so, the effects of planetary waves, tides, and other small-scale waves are largely removed in the mean residual profiles. The daily zonal mean differences between the MIPAS IMK and the transformed GPS-RO/CHAMP JPL temperatures, $\mathbf{x}_{mipas}$ and $\tilde{\mathbf{x}}_{champ}$ are displayed in Figure 5 for the MIPAS

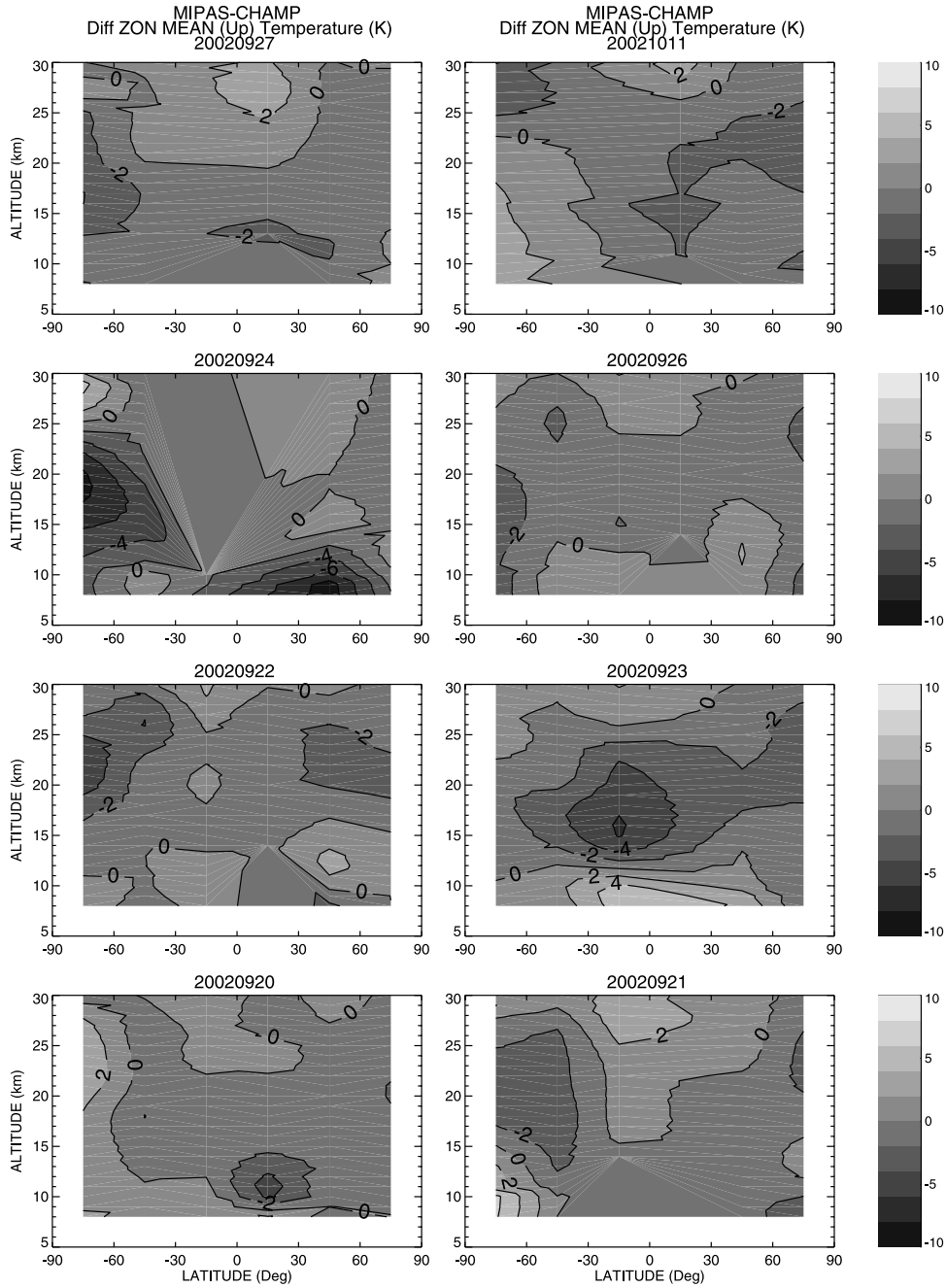

Figure 6. Same as Figure 5, but for MIPAS observations in ascending orbit node (nighttime).

downleg (daytime) and in Figure 6 for the upleg (nighttime) observations during eight days in September/October of 2002. The other days show similar features and are not displayed here. Similar comparisons results for the MIPAS IMK and GPS-RO/CHAMP GFZ data can be found in *Wang et al.* [2004a].

[21] For the eight days, the daily zonal mean differences of $\delta = \mathbf{x}_{mipas} - \tilde{\mathbf{x}}_{champ}$ are less than 1–2 K in large latitude and altitude regions. However, they vary considerably with latitude and altitude, from day to day, and between day and night. There is a tendency for MIPAS temperatures below 25 km to be slightly lower than GPS-RO JPL. In contrast, the MIPAS temperatures above 25 km are higher than those of the GPS-RO JPL. The mean differences are relatively small between 30°S and 90°N, but increase in the region of 30°S and 90°S, with a maximum of 4–6 K. The causes of these large discrepancies will be discussed in section 4.1.

[22] To further reduce the fluctuations observed in the daily zonal means and increase statistical confidence, we examine the 14-day zonal averages of the temperature differences $\delta = \mathbf{x}_{mipas} - \tilde{\mathbf{x}}_{champ}$ for the September/October period (Figure 7). Much better consistency between the MIPAS IMK and GPS-RO/CHAMP JPL temperatures is seen in the 14-day zonal means, in comparison with the daily zonal means in Figures 5 and 6. The 14-day zonal mean differences are generally less than 1 K. Larger discrepancies of ~2 K are seen mainly around the equator and the two poles in the height regions below 10 km and

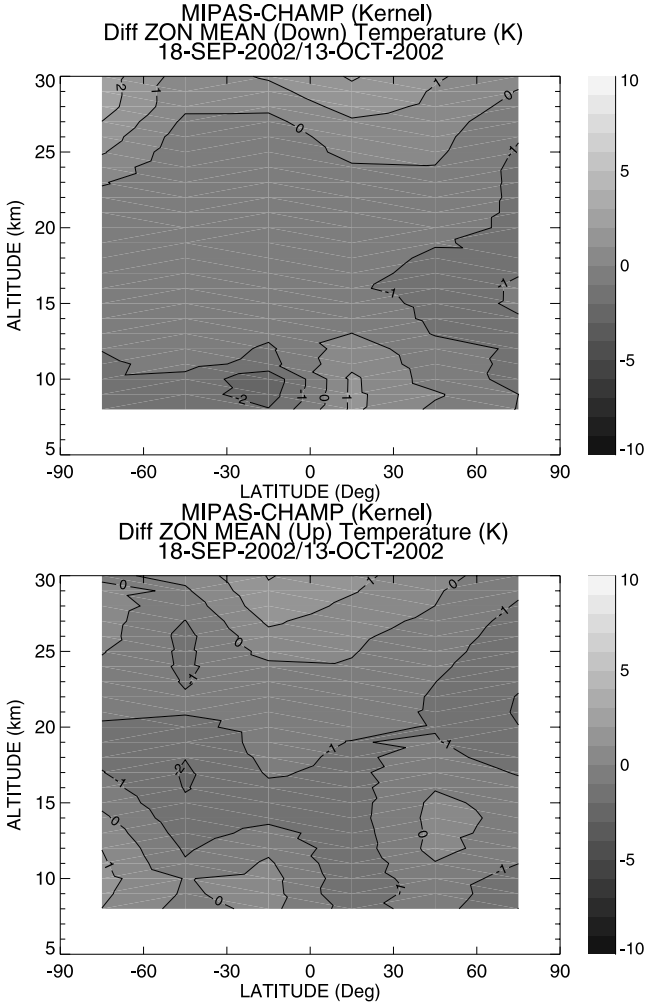

Figure 7. Zonal mean temperature differences between MIPAS IMK and GPS-RO/CHAMP JPL retrievals. Adjustment of altitude resolution and a priori information is applied. The data are averaged over the 14 days of the September/October period (see Table 1) for the MIPAS descending (daytime, top) and ascending (nighttime, bottom) orbit nodes. The temperature contour interval is 1 K.

around 30 km. Also, around 30°S and 15 km, the MIPAS temperatures appear to be lower than GPS-RO/CHAMP JPL during the nighttime observations, but show better consistency during the daytime observations.

[23] Finally, we combined all correlative measurements available for both legs and calculated global mean differences and standard deviations of $\delta = \mathbf{x}_{mipas} - \tilde{\mathbf{x}}_{champ}$ during each day and the 14 days. The daily global mean differences (not shown) are $\Delta(z) \leq 2$ K and the standard deviations $\sigma(z) \simeq 4$ K or more. The 14-day global mean differences are displayed in Figure 8 for the MIPAS/GPS-RO JPL (top) and MIPAS/GPS-RO GFZ (bottom) comparisons. The GPS-RO JPL and GFZ temperatures are seen to be generally consistent with each other and with the MIPAS retrievals. The 14-day global mean differences at each heights are $\Delta(z) \leq 1$ K, and the standard deviations are $\sigma(z) \leq 4$ K. The averages of the 14-day means between 8 and 30 km are −0.44 and 0.07 K for the JPL and GFZ comparison, respectively, and the height-averaged standard deviations are less than 3.5 K. The height-averaged 1-σ uncertainty is 0.02 K. This indicates that the MIPAS IMK temperatures are in very good agreement with the GPS-RO GFZ and has a lower bias of ∼0.5 K with respect to the JPL data. More specifically, there exists a tendency for MIPAS temperatures between 15–25 km to be lower than the GPS-RO/CHAMP JPL and GFZ by less than ∼1 K and ∼0.2 K, respectively. Below 15 km, the MIPAS temperatures tend to be lower than GPS-RO/CHAMP JPL by ∼1 K, but consistent well with GPS-RO/CHAMP GFZ. Above 25 km, the MIPAS temperatures are higher than GPS-RO/CHAMP JPL and

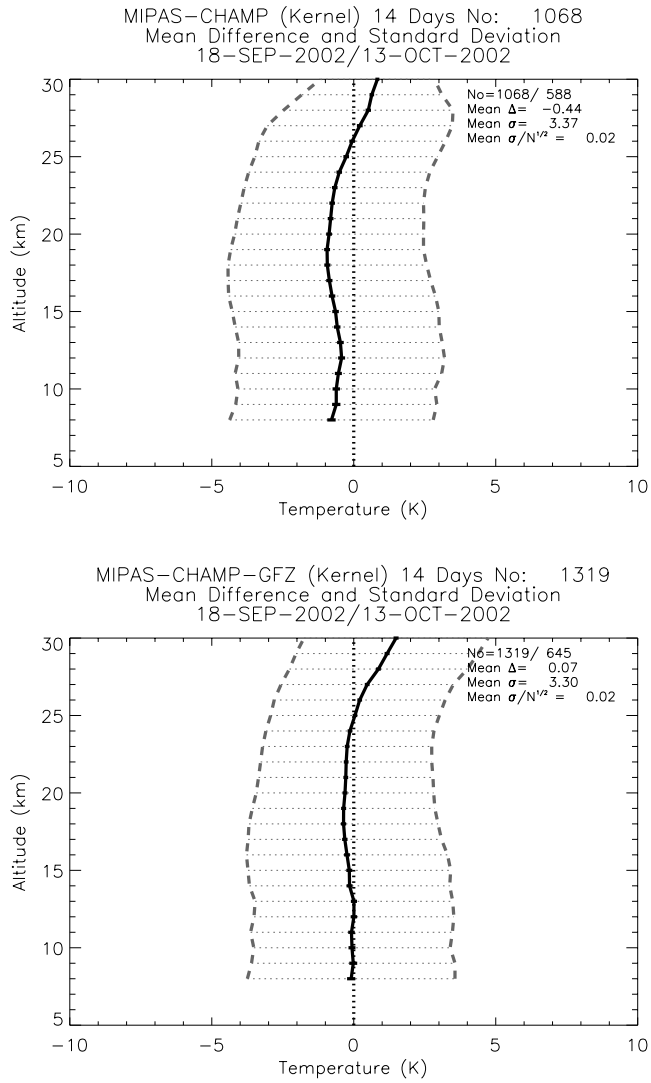

Figure 8. Global mean differences $\Delta(z)$ (solid) and standard deviations $\sigma(z)$ (dotted) of MIPAS IMK temperatures (in Kelvin) with respect to GPS-RO/CHAMP JPL (top) and GFZ (bottom) retrievals. Adjustment of altitude resolution and a priori information is applied. The data are averaged over the 14 days of September/October 2002. Error bars (thick line) represent the 1-σ uncertainty $\sigma(z)/N^{1/2}(z)$ for the 14-day means. The maximum and minimum numbers of data points $N(z)$ at individual heights are denoted, followed by mean values of $\Delta(z)$, $\sigma(z)$, and $\sigma(z)/N^{1/2}(z)$ averaged over all heights.

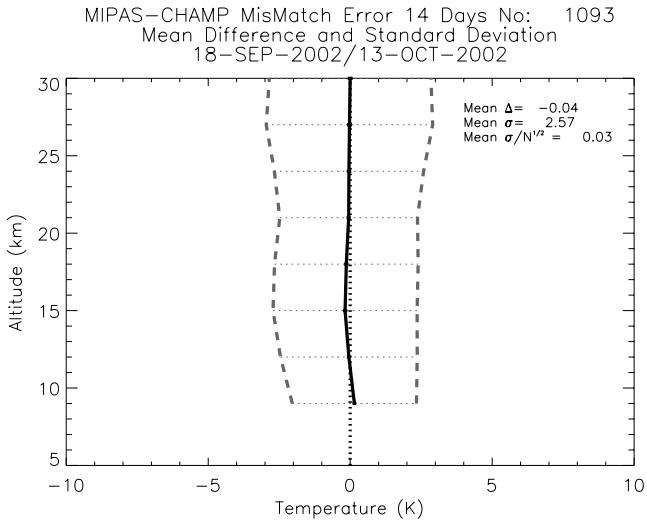

Figure 9. Simulated global mean temperature (in Kelvin) differences (solid) and standard deviations (dotted) due to spatial mismatch between MIPAS and GPS-RO/CHAMP correlative measurements (see section 4.1 for details). Denoted in the panel are the mean values of $\Delta(z)$, $\sigma(z)$, and $\sigma(z)/N^{1/2}(z)$ averaged over all heights.

GFZ, and peaked at 30 km with maximum magnitudes of ~1 K and ~1.5 K, respectively.

4. Discussions

[24] The 14-day mean differences, either the height averaged values of −0.44 K and 0.07 K or the maximum values of 1 K and 1.5 K at 30 km for the MIPAS versus the JPL and GFZ retrievals, respectively, are within the accuracy of the instrument measurements. Even though we do not have access to the GPS retrieval error covariances, their accuracy is known to be typically better than 1 K [e.g., *Hajj et al.*, 2002; *Wickert et al.*, 2004a]. A detailed discussion of the MIPAS retrieval error budget is presented in section 4.5, and the total error for specific profiles at stratospheric altitudes is estimated at 0.5–1.5 K. This means that near the MIPAS tangent altitudes a total error of 1.5–2.5 K is approximately expected for the differences between correlative profiles. In this perspective, the consistency between the three data sets are rather good. Nonetheless, a significant number of comparisons differs more than the expected total error (i.e., the standard deviation of the comparison ensemble is greater than the expected total error). There are significant temporal and spatial variations of 2–4 K or more in magnitude. Some features and possible explanations of the detected variabilities are discussed in this section.

4.1. Effect of Imperfect Match

[25] For comparisons of individual profiles, imperfect spatial/temporal coincidence has significant contributions to the observed discrepancies between MIPAS and GPS-RO temperatures. As shown in Figure 1, the mismatches in horizontal distance and time are minimized in the polar regions, but maximized near the equator. However, in the southern polar region, the horizontal temperature gradients are large, and are significantly enhanced during the major warming in the observation period [e.g., *Manney et al.*, 2004]. Also, near the equator, gravity wave activity is relatively strong, with mean temperature fluctuations of 4–5 K on local spatial scales comparable to our coincidence interval [*Jiang et al.*, 2004b]. These geophysical fluctuations can cause temperature differences on space scales and timescales smaller than the 5° latitude, 10° longitude, and 6 hour coincidence criteria used in our analysis. These discrepancies are expected to be significantly reduced or cancelled out when large ensembles are averaged.

[26] To quantify the effect, we take temperature data at 12:00 UTC from the METO (Met Office, United Kingdom) assimilation analysis, and sample the fields by the MIPAS and GPS-RO/CHAMP observation configurations during the 14 days in September/October 2002. The temperatures at the correlative measurement locations are estimated by interpolating the METO fields. Their differences and standard deviations are calculated and averaged over the 14 days. The simulated mean differences and standard deviations are shown in Figures 9 and 10 for the global

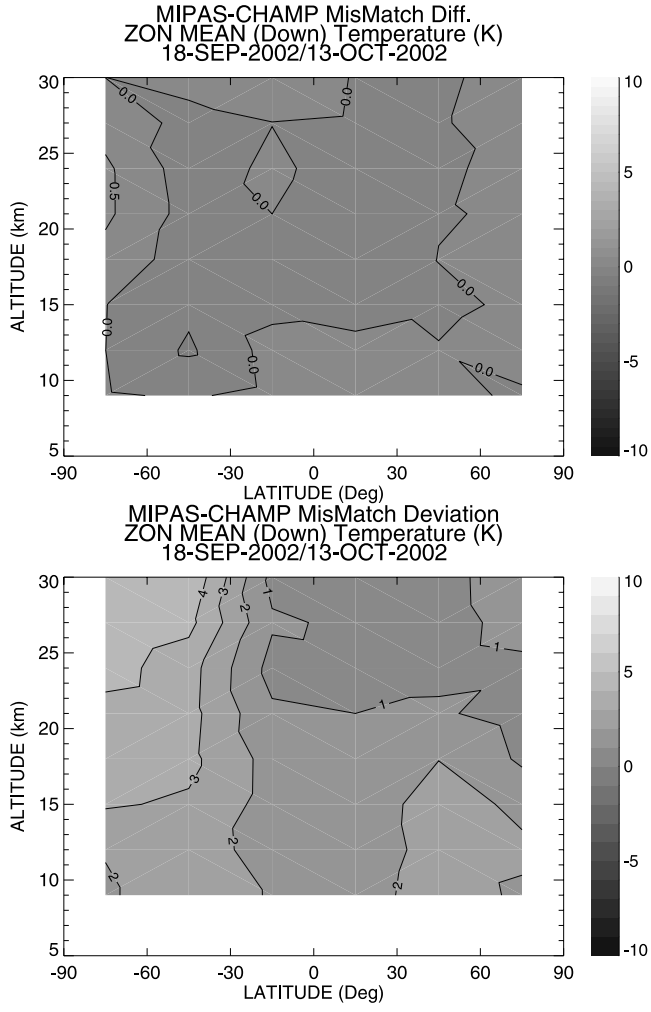

Figure 10. Simulated zonal mean temperature (in Kelvin) differences (top) and standard deviations (bottom) due to spatial mismatch between MIPAS and GPS-RO/CHAMP correlative measurements (see section 4.1 for details). Shown are the results for MIPAS descending (daytime) observations. The difference and standard deviation contour intervals are 0.5 K and 1 K, respectively.

and zonal averages, respectively. The global mean differences are virtually zero with a mean standard deviation of 2.6 K, and have similar values at almost all heights between 8 and 30 km. The zonal mean differences at most altitudes and latitudes are zeros and the standard deviations are 1–2 K. The largest mean differences of 0.5 K and standard deviations of 2–4 K are found between 15 and 30 km in the southern polar regions. This suggests influences of the unusual planetary wave activity during the southern stratospheric major warming and polar vortex split [e.g., *Allen et al.*, 2003], due to imperfect temporal and spatial matching of the correlative profiles.

[27] The above simulation results suggest that imperfect match has no virtual effect on the observed mean differences Δ between the correlative measurements, except for those in the southern polar region. However, the mismatch can significantly contribute to the observed standard deviations σ. Our estimated averaged standard deviation of 2.6 K may only provide a low bound for the σ, since the simulations do not consider geophysical variations in time and in spatial scales smaller than the METO grids (2.5 degrees in latitude and 3.75 degrees in longitude).

4.2. Effect of Vertical Resolution

[28] Different vertical resolutions of the correlative measurements can also have their contributions to the differences calculated by interpolating the data onto a common grid, if there are small-scale temperature structures that are resolved by the high resolution, but not by the low resolution, grid. To account for this effect, we have already adjusted the altitude resolutions by applying the averaging kernel in our comparisons. This eliminates the differences originated from different vertical resolution and a priori (see equation (2) in section 2). Here we try to quantitatively estimate the effect. To do it, we take the differences between the retrieved MIPAS and GPS-RO temperatures, $\mathbf{x}_{mipas} - \mathbf{x}_{champ}$, i.e., no altitude resolution and a priori adjustment is used, compute their mean differences and standard deviations in a manner similar to that described by equations (5) and (6). The 14-day global mean differences and standard deviations for $\mathbf{x}_{mipas} - \mathbf{x}_{champ}$ are exhibited in Figure 11. In comparison with Figure 8 for $\delta = \mathbf{x}_{mipas} - \tilde{\mathbf{x}}_{champ}$ (altitude resolution and a priori adjustment is applied), significant changes are seen only around the tropopause region, where the global means and standard deviations for $\mathbf{x}_{mipas} - \mathbf{x}_{champ}$ exhibit a sharp edge of $\sim$1 K. The unadjusted mean CHAMP temperatures appear to be lower than the adjusted ones by $\sim$1 K. This is consistent with the finding of *Rocken et al.* [1997], and could be a reason for the cold bias of CHAMP. At other heights, the global means for $\mathbf{x}_{mipas} - \mathbf{x}_{champ}$ have no virtual changes in magnitude, but show some small altitude structures, and the standard deviations for $\mathbf{x}_{mipas} - \mathbf{x}_{champ}$ are increased by less than 0.5 K.

[29] The above results show that the differences originated from different vertical resolution and a priori are generally small, except for the tropopause region. This is not surprising. The small structures not resolved by low resolution grid are usually associated with large vertical gradients of the climatological field and/or geophysical perturbations due to planetary waves and gravity waves, as well as tides (though they are thought to be small in the region of interest). Such

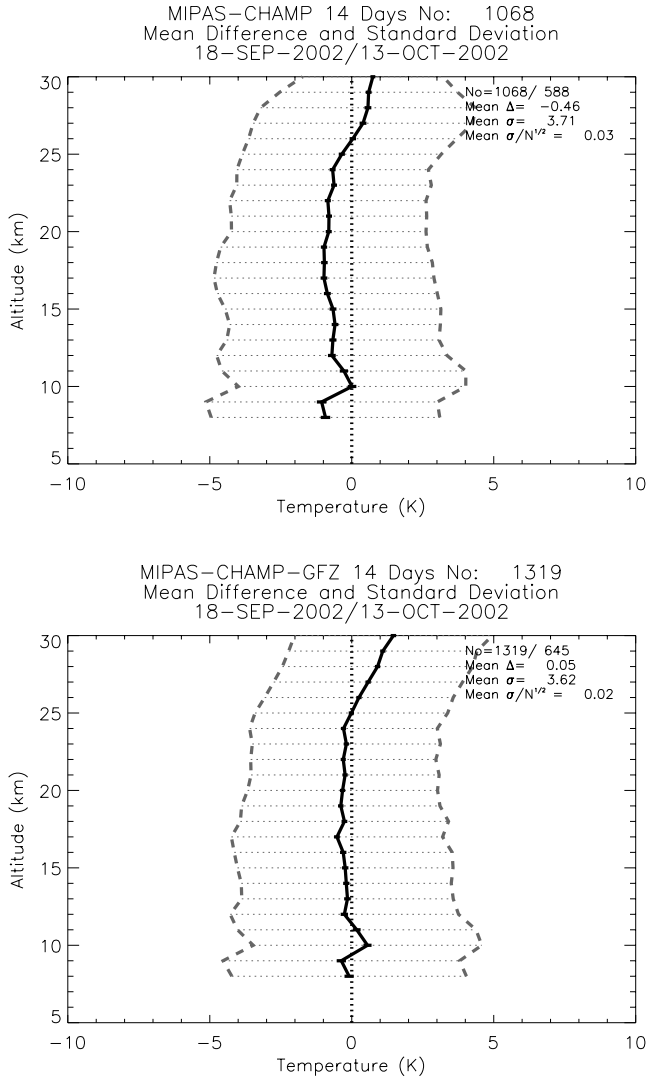

Figure 11. Same as Figure 8, but no adjustment of altitude resolution and a priori information is applied.

structures have their own temporal and spatial variations. Thus, for a statistical analysis of large ensembles taken at different geolocations and times, the influences of such structures on the resultant mean residual profiles are expected to be smoothed or reduced. However, this averaging process is not effective in the tropopause region due to persistent large gradient of the climatological field and coarse resolution of the measurements (see section 3).

4.3. Effect of the a Priori Information

[30] As seen from the 14-day global mean differences in Figure 8, the MIPAS temperatures above 25 km are higher than GPS-RO/CHAMP JPL and GFZ. This tendency increases with increasing height and reaches maximum magnitude of $\sim$0.8 K and $\sim$1.5 K at 30 km for GPS-RO JPL and GFZ data, respectively. The mean difference between GFZ and JPL temperatures is $\sim$0.7 K, comparable to the difference between CHAMP JPL and MIPAS temperatures. The observed differences between GFZ and JPL data sets might be related to the features of the GPS-RO retrievals. As mentioned in section 2, in the current version

of the GFZ and JPL GPS-RO data processor, the derived GPS-RO temperatures depend on the initialization i.e., ECMWF and NCEP temperatures for GFZ and JPL data, respectively, at altitudes near and above 30 km [e.g., *Wickert et al.*, 2001b; *Marquardt et al.*, 2003].

[31] Here we should note the known low bias in the ECMWF temperatures between 30 and 45 km. As pointed out by *Simmons et al.* [2004], the ECMWF loses the radiosonde data and model biases become larger above 30 km. Moreover, the AMSU-A (Advanced Microwave Sounding Unit) data, which the analyses rely on at these levels, are prone to biases also. Recently *Randel et al.* [2002] compared a number of stratospheric climatologies, including one derived from a few years of the ECMWF ERA-40 reanalysis and found that the ECMWF reanalysis stood out as the coldest of all data sets between 30 and 45 km.

[32] We have examined the time series of ECMWF and NCEP temperatures and their differences at 10 hPa (~30 km) and 20 hPa (~25 km) for 18 Sep through 13 October 2002 (not shown here for brevity). At the two height levels, the ECMWF temperatures are generally lower than NCEP at most latitudes. The cold bias of ECMWF increases with increasing height and reaches maximum amplitudes of ~2 K around 29 September and centered about 70°N and 50°S. Thus the deviations between ECMWF and NCEP probably account for the global mean difference of ~1 K at 30 km between GFZ and JPL GPS-RO/CHAMP retrievals. More studies are required and under way to investigate the effect.

4.4. Effect of Water Vapor

[33] The 14-day global mean differences in Figure 11 indicate that the MIPAS temperatures below 10 km tend to be lower than GPS-RO/CHAMP JPL by ~1 K, but generally consistent with or slightly higher than GPS-RO/CHAMP GFZ. This behavior is thought to be mainly associated with a bias in GPS-RO retrievals. Here we should note that the GFZ and JPL data represent "dry" and "wet" temperatures, respectively. The dry temperatures derived from GPS-RO measurements could have a cold bias due to the presence of water vapor [*Wickert et al.*, 2001a].

[34] Water vapor has an important influence on the GPS-RO temperature retrievals. The microwave signals measured by GPS radio occultation are used to derive the bending angle of each ray, which can be inverted to a profile of the refractive index through the Abel transform. At microwave frequencies the refractivity is very sensitive to water vapor, which is present in the troposphere. The GFZ temperatures are derived using the classical dry temperature retrieval [*Wickert et al.*, 2001a]. The JPL retrieval determines (for each profile) the altitude where the water vapor contribution is significant ($T \geq 250$ K). Above this "transition" altitude, the "wet" term in the refractivity is considered negligible. The retrieved temperature will be equal to the "dry temperature." Below this altitude, the water vapor term is solved using the temperature from the NCEP analysis, and the retrieved temperature there will be just the NCEP temperature. (See *Hajj et al.* [2002, 2004] for more details).

[35] For GPS occultations in the troposphere, the "dry temperatures" are usually lower than the "wet temperatures." The difference could be as large as 5 K around 5 km and decreases above. This is because, for the "dry temperature," the "refractivity part of water vapor" is simply and wrongly transformed into additional air density, and "more air density" is equal to "lower temperature" (relative variations of density and temperature are in antiphase). The effect of water vapor may contribute to the observed discrepancies of ~2 K below 10 km around the equator and around 30°S (see Figure 7).

[36] In particular, the effect of water vapor may have significant contribution to the observed standard deviations. As shown by *Tsuda et al.* [2000] and *Jiang et al.* [2004b], at midlatitudes and around the equator, gravity waves are strong. The observed wave variances correspond to mean temperature fluctuations of 4–5 K. *Jiang et al.* [2004b] also show that the upper tropospheric water vapor at these latitudes is higher in correlation with the enhanced wave activities above the major convection centers. The tropical deep convection over land usually acts to moisten the air near the tropopause, while convection over the ocean may dehydrate the tropopause. Both enhanced gravity waves and increased water vapor could introduce larger deviations between correlative MIPAS and GPS-RO temperature measurements. Further studies are required to quantify this effect on the retrieved GPS-RO temperatures. In turn, the temperature and water vapor measurements of MIPAS and GPS-RO/CHAMP will provide valuable information for understanding the dynamical processes affecting climate change in the troposphere and stratosphere.

4.5. Error Budgets

[37] The observed discrepancies between the MIPAS and GPS-RO temperatures are also related to the measurement limitation of individual instruments. A detailed analysis of the error budgets has been reported by *von Clarmann et al.* [2003c] for the MIPAS temperatures and by *Hajj et al.* [2002] and *Wickert et al.* [2004a] for the GPS-RO retrievals. They concluded that, for a single profile, the MIPAS temperatures are retrieved with a total error of 0.5–1.5 K at stratospheric altitudes and the GPS-RO temperatures are derived with an accuracy of typically better than 1 K. For a large ensemble, random error components should average out, but the systematic components do not.

[38] Here we specifically discuss the systematic bias of the MIPAS temperature retrievals due to insufficient knowledge of the instrumental line shape (ILS), which was not addressed in *von Clarmann et al.* [2003c]. In the retrieval algorithm, a model spectrum of the atmospheric signal is simulated by the radiative transfer through the Earth's atmosphere for an optimal instrument with infinitesimal field of view, infinite instrumental spectral resolution and no distortion of the line shape. This spectrum is convolved with the apodised instrument line shape to obtain the apodised spectrum, which includes the effects of finite resolution, line shape distortions and apodization. The information on these effects is provided by Level 1B data processing. At the time of generating the MIPAS version V1.0 data for the September/October 2002, which are used in this comparison study, the knowledge of ILS was insufficient. A linear error assessment has been carried out to estimate the ILS bias.

[39] As an example, Figure 12 displays the estimation of absolute errors for four MIPAS temperature profiles observed on 26 September 2002. The measurements are taken at 80°N, ~2°N, 63°S, and ~2°S. The ILS errors are estimated to be 0.2 to 1.2 K with a significant altitude

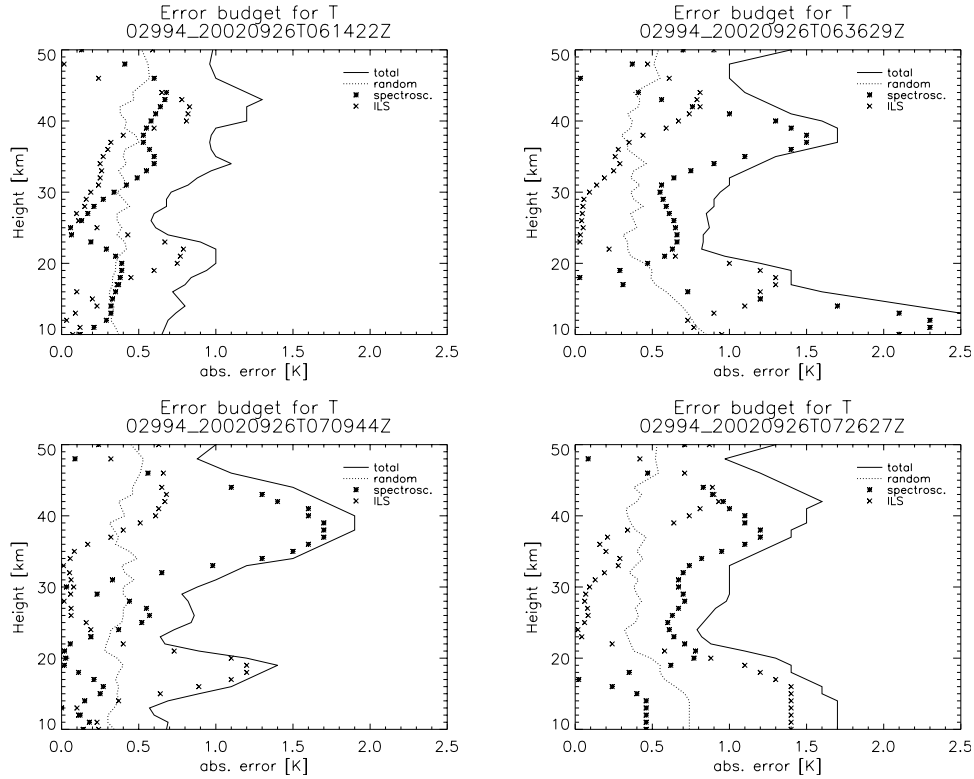

Figure 12. Estimation of absolute error for four MIPAS temperature (in Kelvin) profiles observed on 26 September 2002 at northern (top) and southern (bottom) polar (left) and equatorial (right) regions. The error components contributing to the total error are the instrument line shape (ILS) bias, spectroscopic data uncertainty, measurement noise, and other uncertainties (not shown) of much less importance.

dependence. There are maxima around 20 km and secondary maxima near 40 km, while minima occur around 30 km. In the height regions of the maxima, the ILS bias is the major contribution to the total error budget. Other error components under consideration are measurement noise and spectroscopic data uncertainties. The spectroscopic errors are about 0.1–0.7 K near 30 km, but increase with increasing height and dominate the total error budget above 30 km in most cases, with maximum magnitudes of 1.5 K or more around 40 km.

[40] The ILS and spectroscopic errors are of systematic nature and cannot be removed when further averaging the MIPAS total error for a large ensemble. To see the ILS effects, we compared the temperatures retrieved with the ILS parameters provided from ESA L1B data processing (used throughout this V1.0 version of MIPAS IMK temperatures) with those retrieved using improved ILS parameters. The latter were estimated from specific measurements taken during July 2002 and resembles the latest ESA results. This set of ILS parameters is preferable, because they are constant, not a function of wave number (as should be expected from instrumental parameters of misalignment) and they are self-consistent, as we can guarantee that the same ILS model has been used for this exercise as is used within radiative transfer algorithm (F. Hase, private communication). The differences in both temperatures are shown in Figure 13 for orbit 03244 taken on 13 October 2002. The temperatures with the unproved knowledge on ILS increase by 0.5 K and 0.2 K around 20 and 40 km, respectively, but slightly decrease by less than 0.2 K near 30 km. These features are seen for all latitude bands, suggesting a cold bias around 20 and 40 km, and a weak hot bias near 30 km in the current IMK version V1.0 MIPAS data.

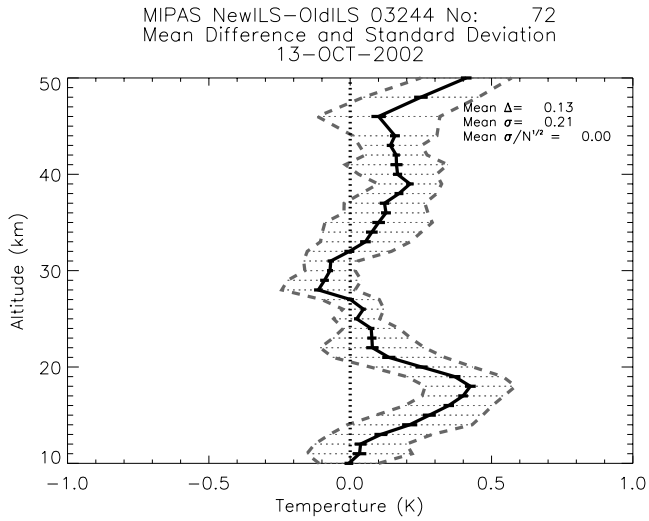

Figure 13. Differences between the MIPAS temperatures retrieved using different instrument line shape (ILS) parameters. The global mean differences are calculated for the 72 profiles of MIPAS orbit 3244 on 13 October 2002. See section 4.5 for details.

[41] As discussed in section 4.4, the GFZ CHAMP "dry" temperatures have a cold bias in comparison with the JPL "wet" temperatures. However, the MIPAS temperatures are closer to GFZ than JPL (see Figure 8). One may raise a question why this is so if JPL CHAMP temperatures are "more correct" because they take water vapor into account. The cold bias due to the ILS error in the current MIPAS retrievals around 20 km may provide an explanation. After application of the corrected ILS, the new MIPAS temperatures are expected to be higher by 0.5 K in the height region, leading to better agreement with the JPL measurements, but will show a hot bias of 0.5 K with respect to the GFZ data.

[42] Also, the current MIPAS temperatures near 30 km will be lower by 0.2 K after application of the corrected ILS, improving the agreements with both GFZ and JPL GPS-RO/CHAMP measurements. However, since there exist the global mean differences of 1 K and 1.5 K for the current MIPAS retrievals with respect to the JPL and GFZ data near 30 km, a decrease of less than 0.2 K in the MIPAS temperatures at that height is most unlikely to overturn our discussions in the section 4.3.

5. Conclusions

[43] More than 1000 profiles of the MIPAS IMK and GPS-RO/CHAMP JPL and GFZ temperature measurements during 14 days of September/October 2002 are compared. The three data sets show generally good agreement in the upper troposphere and lower stratosphere. The 14-day mean differences averaged globally and over height region between 8 and 30 km are estimated as -0.44 ± 0.02K and 0.07 ± 0.02K, with maximum biases of 1 K and 1.5 K at 30 km for MIPAS/GPS-RO JPL and GFZ comparisons, respectively. These biases are within the expected total error of 1.5–2.5 K for the differences between correlative profiles due to accuracy of the instrument measurements.

[44] However, the observed differences between the correlative measurements show altitude, latitude, and day-night, as well as day-to-day variations with a standard deviations of 2–4 K, implying that a significant number of comparisons differs more than the expected total error. Some features of note are as follows:

[45] 1. Between 15 and 25 km, MIPAS temperatures are slightly lower than the GPS-RO/CHAMP JPL and GFZ by less than 1 K and 0.2 K, respectively.

[46] 2. Below 15 km, the MIPAS temperatures tend to be lower than GPS-RO/CHAMP JPL by ~1 K, but consistent well with GPS-RO/CHAMP GFZ.

[47] 3. Above 25 km, the MIPAS temperatures are higher than GPS-RO/CHAMP JPL and GFZ, and peaked at 30 km with maximum magnitudes of ~1 K and 1.5 K, respectively.

[48] 4. Larger discrepancies between the IMK MIPAS and GPS-RO/CHAMP temperatures occur around the equator, 30°S, and the south pole, as well as at the time when the southern polar vortex temporarily broke down during the major warming. The zonal mean differences in this region are ~1–2 K on average over the 14 days.

[49] Several explanations of these observed discrepancies have been found. The effect of imperfect spatial/temporal match between the correlative profiles was shown to be virtually zero for global mean differences (see section 4.1). However, large horizontal temperature gradients in the polar region and during a period of strong planetary wave activity can be mapped into the difference residuals. Similarly, enhanced gravity wave activity near the equator and at midlatitudes could also introduce larger discrepancies. Due to the effect of imperfect match in these latitudinal regions, the standard deviations are estimated at least as 2.6 K or ~80% of the 3.3 K observed mean standard deviations.

[50] The implementation detail of the initial temperature setup at the upper level seems to have significant influence on the GPS-RO retrievals in the midstratosphere (see section 4.3). The effect can be tracked even down in the lower stratosphere or tropical tropopause. Increased humidity near and below the tropopause results in a low bias in the retrieved GPS-RO temperatures. Increased water vapor associated with the deep convection in the tropical tropopause region could also introduce large standard deviations (see section 4.4).

[51] The MIPAS IMK version V1.0 data used for this analysis were produced with insufficient knowledge of instrumental line shape. This introduced a systematic cold bias of 0.5 K and 0.2 K around 20 km and 40 km, respectively, and a weak hot bias of ~0.2 K near 30 km in the current MIPAS temperatures (see section 4.5). Thus application of correct ILS is expected to further improve the consistency between the MIPAS and GPS-RO/CHAMP measurements at both height regions. However, a decrease of 0.2 K in the MIPAS temperatures near 30 km cannot alter our discussions about the global mean differences of 1 K and 1.5 K at that height for the current MIPAS retrievals with respect to the JPL and GFZ data, respectively.

[52] Finally, we note that the altitude resolutions of the comparison data sets have been adjusted by applying the averaging kernel. If one wants to compare the unadjusted data sets, different vertical resolution of the correlative measurements can contribute to the observed discrepancies, in particular in the tropopause region. The vertical structures of temperature field near the tropopause could be resolved by the higher resolution measurements (GPS-RO), but not by the lower ones (MIPAS). This may introduce ~1 K bias in the observed mean differences between the correlative profiles, and ~0.5 K bias in the observed mean standard deviations (see section 4.2). These values are referred to the tropopause only.

[53] **Acknowledgments.** We are grateful to ESA for providing us with MIPAS Level-1B data during the commissioning phase. The METO (Met Office, United Kingdom) stratospheric assimilation data are provided through BADC (British Atmospheric Data Centre). The research work of IMK-IAA MIPAS group has been funded by EC via contract EVG1-CT-1999-00015 (AMIL2DA), BMBF via project 07 ATF 43/44 (KODYACS), 07 ATF 53 (SACADA), and 01 SF 9953 (HGF-VF), and ESA via contract 15530/01/NL/SF (INFLIC). The IAA team was partially supported by Spanish projects PNE-017/2000-C and REN2001-3249/CLI. B. Funke has been supported through a European Community Marie Curie Fellowship. The authors also acknowledge the support by the Jet Propulsion Laboratory, California Institute of Technology, under contract with the National Aeronautics and Space Administration of the United States.

References

Allen, D. R., R. M. Bevilacqua, G. E. Nedoluha, C. E. Randall, and G. L. Manney (2003), Unusual transport and mixing during the 2002 Antarctic winter, *Geophys. Res. Lett.*, *30*, 1599, doi:10.1029/2003GL017117.

Ao, C. O., W. B. Schreiner, and J. Wickert (2003), First report on the CHAMP Radio Occultation Intercomparison Study, *JPL Publ.*, *03-016*.

Bevington, P. R. (1969), *Data Reduction and Error Analysis for the Physical Sciences*, McGraw-Hill, New York.

European Space Agency (ESA) (2000), Envisat: MIPAS, An instrument for atmospheric chemistry and climate research, *Spec. Publ. ESA-SP-1229*, Eur. Space Res. and Technol. Cent., Noordwijk, Netherlands.

Fischer, H., and H. Oelhaf (1996), Remote sensing of vertical profiles of atmospheric trace constituents with MIPAS limb emission spectrometers, *Appl. Opt.*, *35*(16), 2787–2796.

Gorbunov, M. E., and S. V. Sokolovskiy (1993), Remote sensing of refractivity from space for global observations of atmospheric parameters, *Tech. Rep. 119*, Max-Planck-Inst. für Meteorol., Hamburg, Germany.

Hajj, G. A., E. R. Kursinski, L. J. Romans, W. I. Bertiger, and S. S. Leroy (2002), A technical description of atmospheric sounding by GPS occultation, *J. Atmos. Sol. Terr. Phys.*, *64*, 451–469.

Hajj, G. A., C. O. Ao, B. A. Iijima, D. Kuang, E. R. Kursinski, A. J. Mannucci, T. K. Meehan, L. J. Romans, M. de la Torre Juarez, and T. P. Yunck (2004), CHAMP and SAC-C atmospheric occultation results and intercomparisons, *J. Geophys. Res.*, *109*, D06109, doi:10.1029/2003JD003909.

Hocke, K. (1997), Inversion of GPS meteorology data, *Ann. Geophys.*, *15*, 443–450.

Jiang, J. H., et al. (2004a), Comparison of GPS/SAC-C and MIPAS/ENVISAT temperature profiles and its possible implementation for EOS MLS observations, in *Earth Observation With CHAMP: Results From Three Years in Orbit*, edited by C. Reigber et al., pp. 573–578, Springer-Verlag, New York.

Jiang, J. H., B. Wang, K. Goya, K. Hocke, S. D. Eckerman, J. Ma, D. L. Wu, and W. G. Read (2004b), Geographical distribution and interseasonal variability of tropical deep convection: UARS MLS observations and analyses, *J. Geophys. Res.*, *109*, D03111, doi:10.1029/2003JD003756.

Kursinski, E. R., G. A. Hajj, K. R. Hardy, J. T. Schofield, and R. Linfield (1997), Observing Earth's atmosphere with radio occultation measurements using the Global Positioning System, *J. Geophys. Res.*, *102*, 23,429–23,465.

Manney, G. L., J. L. Sabutis, D. R. Allen, W. A. Lahoz, A. A. Scaife, S. Pawson, C. E. Randall, B. Naujokat, and R. Swinbank (2004), Simulations of dynamics and transport during the September 2002 Antarctic major warming, *J. Atmos. Sci.*, in press.

Marquardt, C., K. Schöllhammer, G. Beyerle, T. Schmidt, J. Wickert, and C. Reigber (2003), Validation and data quality of CHAMP radio occultation data, in *First CHAMP Mission Results for Gravity, Magnetic, and Atmospheric Studies*, edited by C. Reigber, H. Lühr, and P. Schwintzer, pp. 384–396, Springer-Verlag, New York.

Melbourne, W. G., E. S. Davis, C. B. Duncan, G. A. Hajj, K. R. Hardy, E. R. Kursinski, T. K. Meehan, L. E. Young, and T. P. Yunck (1994), The application of spaceborne GPS to atmosphere limb sounding and global change monitoring, *JPL Publ.*, *94-18*.

Palmer, P., J. Barnett, J. Eyre, and S. Healy (2000), A nonlinear optimal estimation inverse method for radio occultation measurements of temperature, humidity, and surface pressure, *J. Geophys. Res.*, *105*(D13), 17,513–17,526.

Randel, W. J., M.-L. Chanin, and C. Michaut (2002), SPARC intercomparison of middle atmosphere climatologies, *SPARC Rep. 3*, Stratos. Processes and Their Role in Clim., Geneva.

Rocken, C., et al. (1997), Analysis and validation of GPS/MET data in the neutral atmosphere, *J. Geophys. Res.*, *102*(D25), 29,849–29,866.

Rodgers, C. D., and B. J. Connor (2003), Intercomparison of remote sounding instruments, *J. Geophys. Res.*, *108*(D3), 4116, doi:10.1029/2002JD002299.

Simmons, A., M. Hortal, G. Kelly, A. McNally, A. Untch, and S. Uppala (2004), ECMWF analyses and forecasts of stratospheric winter polar vortex break-up: September 2002 in the southern hemisphere and related events, *J. Atmos. Sci.*, in press.

Spang, R., J. J. Remedios, and M. P. Barkley (2004), Colour indices for the detection and differentiation of cloud types in infra-red limb emission spectra, *Adv. Space Res.*, *33*(7), 1041–1047.

Steck, T. (2003), Intercomparison of AMIL2DA results for MIPAS-ENVISAT data, task report, contract EVG1-CT-1999-00015 (AMIL2DA), Eur. Comm., Brussels.

Steiner, A. K., G. Kirchengast, and H. P. Ladreiter (1999), Inversion, error analysis, and validation of GPS/MET data, *Ann. Geophys.*, *17*, 122–138.

Stiller, G. P., T. Steck, M. Milz, T. von Clarmann, U. Grabowski, and H. Fisher (2003a), Approach to the cross-validation of MIPAS and CHAMP temperature and water vapor profiles, in *First CHAMP Mission Results for Gravity, Magnetic, and Atmospheric Studies*, edited by C. Reigber, H. Lühr, and P. Schwintzer, pp. 550–556, Springer-Verlag, New York.

Stiller, G. P., et al. (2003b), Early IMK/IAA MIPAS/ENVISAT results, in *Remote Sensing of Clouds and the Atmosphere VII*, edited by K. Schäfer and O. Lado-Bordowsky, *Proc. SPIE*, *4882*, 184–193.

Thayer, G. (1974), An improved equation for the radio refractive index of air, *Radio Sci.*, *9*(10), 803–807.

Tsuda, T., M. Nishida, C. Rocken, and R. Ware (2000), A global morphology of gravity wave activity in the stratosphere revealed by the GPS occultation data (GPS/MET), *J. Geophys. Res.*, *105*, 7257–7273.

von Clarmann, T., et al. (2003a), Remote sensing of the middle atmosphere with MIPAS, in *Remote Sensing of Clouds and the Atmosphere VII*, edited by K. Schäfer and O. LadoBordowsky, *Proc. SPIE*, *4882*, 172–183.

von Clarmann, T., et al. (2003b), A blind test retrieval experiment for infrared limb emission spectrometry, *J. Geophys. Res.*, *108*(D23), 4746, doi:10.1029/2003JD003835.

von Clarmann, T., et al. (2003c), Retrieval of temperature and tangent altitude pointing from limb emission spectra recorded from space by the Michelson interferometer for passive atmosphere (MIPAS), *J. Geophys. Res.*, *108*(D23), 4736, doi:10.1029/2003JD003602.

Wang, D. Y., et al. (2004a), Comparisons of MIPAS/ENVISAT and GPS-RO/CHAMP temperature profiles, in *Earth Observation With CHAMP: Results From Three Years in Orbit*, edited by C. Reigber et al., pp. 567–572, Springer-Verlag, New York.

Wang, D. Y., et al. (2004b), Comparisons of MIPAS-observed temperature profiles with other satellite measurements, in *Remote Sensing of Clouds and the Atmosphere VIII*, edited by K. P. Schäfer et al., *Proc. SPIE*, *5235*, 196–207.

Ware, R., et al. (1996), GPS sounding of the atmosphere from low Earth orbit: Preliminary results, *Bull. Am. Meteorol. Soc.*, *77*, 19–40.

Wickert, J., et al. (2001a), GPS ground station data for CHAMP radio occultation measurements, *Phys. Chem. Earth (A)*, *26*, 503–511.

Wickert, J., et al. (2001b), Atmosphere sounding by GPS radio occultation: First results from CHAMP, *Geophys. Res. Lett.*, *28*(17), 3263–3266.

Wickert, J., et al. (2003), GPS radio occultation with CHAMP: First comparison of analysis results from GFZ, JPL, and UCAR, EGS-AGU-EUG Joint Assem., Nice, France, 6–11 April.

Wickert, J., T. Schmidt, G. Beyerle, R. König, C. Reigber, and N. Jakowski (2004a), The radio occultation experiment aboard CHAMP: Operational data analysis and validation of vertical atmospheric profiles, *J. Meteorol. Soc. Jpn.*, *82*(1B), 381–395.

Wickert, J., T. Schmidt, G. Beyerle, G. Michalak, R. König, J. Kaschenz, and C. Reigber (2004b), Atmospheric profiling with CHAMP: Status of the operational data analysis, validation of the recent data products and future prospects, in *Earth Observation With CHAMP: Results From Three Years in Orbit*, edited by C. Reigber et al., pp. 495–500, Springer-Verlag, New York.

C. O. Ao, J. H. Jiang, G. Manney, L. J. Romans, and D. L. Wu, Jet Propulsion Laboratory, California Institute of Technology, Pasadena, CA 91109, USA.

H. Fischer, N. Glatthor, U. Grabowski, M. Höpfner, S. Kellmann, M. Kiefer, A. Linden, M. Milz, T. Steck, G. P. Stiller, G. M. Tsidu, T. von Clarmann, and D.-Y. Wang, Institut für Meteorologie und Klimaforschung (IMK), Forschungszentrum Karlsruhe GmbH und Universität Karlsruhe, Postfach 3640, 76021 Karlsruhe, Germany. (ding-yi.wang@imk.fzk.de)

B. Funke and M. López-Puertas, Instituto de Astrofísica de Andalucía, CSIC, Apartado Postal 3004, 18008 Granada, Spain.

K. Hocke, Max-Planck-Institut für Aeronomie, 37191 Katlenburg-Lindau, Germany.

T. Schmidt and J. Wickert, Department 1: Geodesy and Remote Sensing, GeoForschungsZentrum Potsdam (GFZ), Telegrafenberg, 14473 Potsdam, Germany.